Large scale self-organisation of 2D hexagonal Ge and Au nanodots on patterned TiO 2

Thomas Bottein, Mohammed Bouabdellaoui, Jean-Benoit Claude, Luc Favre, Thomas David, Magali Putero, Antoine Ronda, Marco Abbarchi, Isabelle Berbezier, David Grosso

Large scale self-organisation of 2D hexagonal Ge and Au nanodots on patterned TiO_2

Thomas Bottein,[†] Mohammed Bouabdellaoui,[†,‡] Jean-Benoît Claude,[†] Luc Favre,[*,†] Thomas David,[†] Magali Putero,[†] Antoine Ronda,[†] Marco Abbarchi,[†] Isabelle Berbezier,[†] and David Grosso[†]

†*Aix Marseille Univ, Université de Toulon, CNRS, IM2NP, Marseille, France*

‡*Laboratory of Physics of Condensed Matter and Renewable Energy, Faculty of Sciences and Technology, Hassan II University of Casablanca, Morocco*

E-mail: luc.favre@im2np.fr

Phone: +33 (0)4 91 28 91 59. Fax: +33 (0)4 91 28 91 61

Abstract

We report a new strategy for the ordering of 2D arrays of Ge and Au nanodots on a silicon wafer using a patterned titanium oxide layer. In a first step, a TiO_2 layer is prepared by block-copolymer-micelles-assisted sol-gel deposition on a full Si wafer, followed by a thermal annealing. The process leads to hexagonally positioned perforations of homogeneous size and spacing. In a second step, these TiO_2 Inorganic NanoPatterns (INPs) are used as templates for the organization of Ge and Au nanodots. Germanium adatoms deposited by Molecular Beam Epitaxy on INPs, diffuse and self-assemble into nanodots, located within the INPs pores. They form homogeneous sub-20 nm Ge nanodots in epitaxy on the silicon substrate and regularly distributed with one dot per perforation. The same approach is used for the formation of Au nanodots. In this case, a gentle mechanical polishing is requiered to suppress the dots seating at

the top of the TiO_2 network. The process developed in this study paves the way to the large scale self-organisation of quantum dots that are highly interesting for various applications, such as opto-electronics, and microelectronics.

Keywords

self-organisation, nanodots, gold, germanium, sol-gel, epitaxy

1 Introduction

In recent years, much attention has been paid to self-organization processes in a large variety of disciplines. Amongst them, several studies have been dedicated to the self-organization of nanostructures (3D, 2D, 1D or 0D) with the aim of fabricating regular arrays of nano-objects assembled in metamaterials with novel functionalities and properties. For instance, metallic nanodots (mainly platinum, silver and gold) are already used in a large number of applications such as nanowires growth catalyst,[1–3] or plasmonics with Surface Enhanced Raman Scattering.[4] On the other hand, 3D semiconductor nanocrystals have been proposed to overcome the limitations of conventional non-volatile memories. Such nanostructures have also attracted much interest as they display quantum size effects that can open the way to new applications in optoelectronics[5] and nanoelectronics.[6] In particular, self-organized islands of Ge on Si are of particular interest as this system is fully compatible with the microelectronic industry. In this context, metallic and semi-conductor nanoparticles are of high interest. However, up to now, the lack in control over the arrangement and size distribution of such objects have limited their applications. The fundamental self-organization mechanism is commonly based on non-linear dynamics of building blocks that self-assemble into larger systems under the combined action of external and internal forces. The building blocks explore various states space until the formation of a preferential center, which precludes the motion of the components independently. We can cite for instance the self-organization using

surface features (steps, kinks, impurities, strain and composition heterogeneities etc.) during evaporation of a foreign material on a substrate. The evaporated material diffuses on the surface and aggregates on the preferential sites of the surface. Such mechanism involves the combination of thermodynamic and kinetic driving forces compelling the motion of material to a special site.

Various strategies have been proposed to obtain 2D arrays of metallic dots of less than 100 nm in diameter with a small size distribution.[7–9] For instance, Choi et al.[7] showed nicely organized Au dots of (30 ± 5) nm in diameter: by using laser interference lithography patterning, silicon oxide is locally removed by wet etching followed by gold deposition. After annealing and lift-off of the photoresist, gold dots are left only in the etched areas with one dot per pit. In addition, direct lithography techniques have also been demonstrated to produce similar results with highly organized sub-100 nm Au dots[10] however these processes are unfortunately more or less cumbersome with various resist patterning and etching steps impractical for scaling over large surfaces.

In the case of semiconductor materials (i.e. Si or Ge), new techniques have been developed to obtain organized semiconductor NPs such as the local removal of a thin silicon oxide layer with an STM tip followed by selective deposition of Ge by reaction between Si and gaseous GeH_4.[11] Other strategies such as nanopatterning using substrate misfit dislocations[12] or self-patterning using vicinal substrates[13–16] have also been explored but a compromise needs to be found between organization and size distribution of the particles. A simple alternative to obtain silicon nanodots is to pattern a resist with the desired design then transferring them to the silicon substrate.[17] However, these techniques are limited to amorphous or polycrystalline objects with dimensions of more than 100 nm.

jFor those reasons, templated dewetting of thin films have attracted much attention as it allows to obtain sub-100 nm, organized nanoparticles.[9] For metallic thin layers, any means used for standard nanofabrication can be applied to fabricate patterned surfaces and direct dewetting for instance electrochemically self-organised surfaces (Al, Ti or Ta),[9,18] organized

nanoperforated layers,[19,20] direct or nanoimprint lithography[21,22] or silicon etching.[23] In the case of semiconductor materials, complex dewetting processes resulting from anisotropic and slow surface diffusion require high dewetting temperatures and defect-free ultra-high vacuum chamber. The formation of islands by solid state dewetting with a good control in size has been shown for simple squared arrays of silicon using FIB or e-beam lithography.[24–26] Very recently, Naffouti *et al* demonstrated the formation of extremely complex silicon patterns with an excellent control over the size distribution by pre-patterning a silicon thin layer with simple shapes.[27,28] However, this degree of organization is always achieved at great expenses using direct lithography techniques with obvious limitation to small scales, far from industrial requirements.

On the other hand, surface patterning through self-assembly of organic[29] and/or inorganic[30] materials using liquid deposition techniques are cheap and easy to implement on large scales. Those self-assembled surfaces can be prepared on a variety of substrates. Even if they suffer from poor long-range ordering and local defects, they are a good alternative to standard lithography techniques to pre-pattern surfaces. A good example of this approach is nanosphere lithography in which organic or inorganic spheres are deposited on a surface where they self-assemble to form organized structures.[31,32] This network can then be used as a mask to obtain periodic nanostructures. Another approach uses electrochemically self-organized surfaces (anodized titania or alumina) as a direct mask[33] or after transfer in silicon by Reactive Ion Etching.[18] Nevertheless, in contrast with metallic particles, those techniques have not yet been proven efficient for the organization of semiconductor nanoparticles. In this paper, we use self-assembled inorganic nanopatterns (INPs) on silicon wafers as templated surfaces. These where prepared by sol-gel liquid deposition of a hybrid solution composed of block copolymer micelles and inorganic metal oxide precursors, in specific conditions where a single layer of hexagonally arranged micelles surrounded by the inorganic precursors is formed on the substrate surface by Evaporation Induced Self-Assembly (EISA).[34] After inorganic condensation and block-copolymer decomposition by heat treatment, the final thin

metal oxide layer bears uniform nano perforations at the micelles formal position, through which the surface of the substrate is accessible.[35] This thin layer can be tailored in terms of thickness from 5 nm to 15 nm, perforation size and spacing from 510 nm to 100 nm by using block-copolymers with different chain length,[36] and in term of composition by changing the precursor source (e.g. TiO_2, SiO_2, ZnO, $CaTiO_3$). Those unique systems have already shown their potential for a number of applications in domains of micropatterning with X-ray lithography,[37] as nanomasks for dry etching,[38] as patterns surfaces for controlled wetting,[34] as photocatalytic surfaces,[39] to create arrays of nanoelectrodes,[40] as electrodes for Hybrid-LEDs,[41] or as template to make magnetic[42] and photomagnetic nanodots[43,44] by liquid deposition. Interestingly, TiO_2 INPs have been previously used to direct solid state dewetting. In this case, a thin layer of germanium was deposited in ultra-high vacuum at room temperature and dewetted at 450 °C. The resulting substrate showed Ge nanodots of about 20 nm in size randomly dispersed onto the TiO_2 surface. Size distribution was reduced compared to non-patterned surfaces and interesting photoluminescence results were obtained.[19] However, no organization was found highlighting the difficulty of directing the growth and dewetting of semiconductor NPs.

Here we report a method to obtain large surfaces of highly organized metallic and semiconductor nanodots through a double self-assembly procedure using the latter TiO_2 INPs as surface templates. In appropriate conditions, such layers display topographical and chemical inhomogeneity between the TiO_2 network and the perforation bottom surface (the substrate surface). These unique features are exploited to direct the solid state dewetting of gold and germanium thin layers within the bottom of perforations. Precise 2D hexagonal arrangements of Ge and Au nanodots with narrow size distribution can be achieved on a scale of several centimeters with size and periodicity previously defined by the INPs characteristics. In addition, in the case of Ge, monocrystalline particles are obtained in epitaxy with the silicon substrate. Such 2D arrays of highly organized nanodots are foreseen to display interesting properties for Surface Enhanced Raman Scattering (SERS), VLS growth catalyst in

the case of metals and as memories or quantum dots for semiconductors.

2 Experimental section

Sol-gel initial solutions are composed of 1 $TiCl_4$; 40 EtOH; 7 H_2O; 1.5×10^{-3} $PB_{12.5}$ – b-PEO_{15} molar ratios. $PB_{12.5}$ – b-PEO_{15} refers to polybutadiene-block polyethylene oxide with blocks of 12 500 and 15 000 $g\,mol^{-1}$. In the case of $PB_{5.5}$ – b-PEO_{30}, the molar ratio is 10^{-3}. The solution is divided in two parts: in part A, PB – b-PEO is dissolved in 2/3 of the ethanol and water; part B contains $TiCl_4$ and the remaining ethanol. The solutions are aged for 2 h at 70 °C then part A is slowly cooled down to room temperature in about 30 min. Finally, both parts are mixed together before use. Films are deposited on cleaned silicon wafer by dip coating at a temperature of 40 °C and a relative humidity below 20 %, using a withdrawal speed ranging between 1 and 3 $mm\,s^{-1}$ in order to obtain a film thickness of less than 10 nm. The resulting film is then annealed at 450 °C for 30 min.

Substrates, previously dip-coated to obtain self-assembled perforations, are immersed into a diluted hydrofluoric acid (HF) solution of 1.17 $mol\,l^{-1}$ for 20 s in order to remove the native silicon oxide at the bottom of the perforations and reveal the silicon surface without damaging the INPs. Open perforations of (28 ± 4) nm in diameter are obtained with accessibility of the substrate surface.

Immediately after HF treatment, the INP substrates are placed under vacuum. Gold is deposited by sputtering at room temperature T_R ($P = 4 \times 10^{-6}$ mbar). Germanium deposition is carried out with an effusion cell ($T_{\text{Ge cell}} = 1150$ °C, deposition speed: 12.62 Å min^{-1}) by Molecular Beam Epitaxy (Riber 32) in ultra-high vacuum (UHV) at a base pressure of 10^{-11} torr. Before deposition, the substrate is heated in the MBE at 450 °C to remove any remaining impurities.

Morphological characterization of the resulting films is obtained by Atomic Force Microscopy (AFM) (PSIA XE-100 AFM) and high resolution Scanning Electron Microscopy

(SEM) (Dual-beam FIB HELIOS 600). Conventional and High Resolution Transmission Electron Microscopy (HRTEM), using FEI Tecnai G2, give structural, chemical and morphological information of the whole system. Refractive index and thickness of the template layers, before Ge deposition, are measured by spectroscopic ellipsometry (Woollam M2000V) using a Cauchy model for dielectric films. X-ray Diffraction (XRD) patterns are recorded on a conventional diffractometer in Bragg-Brentano geometry (PANalytical Empyrean) using Cu radiation ($\lambda = 0.154\,\mathrm{nm}$), a rapid detector (PANalytical PIXcel) and an offset of 4° to avoid Si substrate contribution. Grazing Incidence XRD (GIXRD) analyses are performed with the same set-up with a parallel plate collimator 0.27° at two different incident angles ($\omega = 1°$ and 1.6°) and different in plane angle measured from the Si substrate [0 1 0] direction ($\varphi = 45°$ to 60°). Before any analysis, the sample is carefully oriented with the Si (0 0 1) perpendicular to the diffraction plane.

3 Results and discussion

The strategy used to prepare the organized nanodot arrays is illustrated in Figure 1, together with the SEM images of the bare INP surface (b) and the final nanodots arrays embedded within the perforations (c). As described in the experimental part, a self-assembled network of micelles embedded in a titania sol-gel matrix is deposited by dip-coating on a silicon wafer substrate, forming the intermediate hybrid NanoPatterns (INPs) (Figure 1a). After annealing, a network of circular perforations, in place of the micelles, is obtained through decomposition of the organic copolymers and densification, crystallization and diffusive sintering of the inorganic TiO_2 network.[36] The surface of the substrate is clearly visible through the perforations (see Figure 1b). The nanoperforations of the titania layer form a compact hexagonal lattice on a length scale of few micrometres while, at a larger scale, hexagonal domains with different orientations are found. With the copolymer $PB_{12.5k}$–b-PEO_{15k}, perforations have a diameter of $(20 \pm 3)\,\mathrm{nm}$ with a spacing of 40 nm between perforations

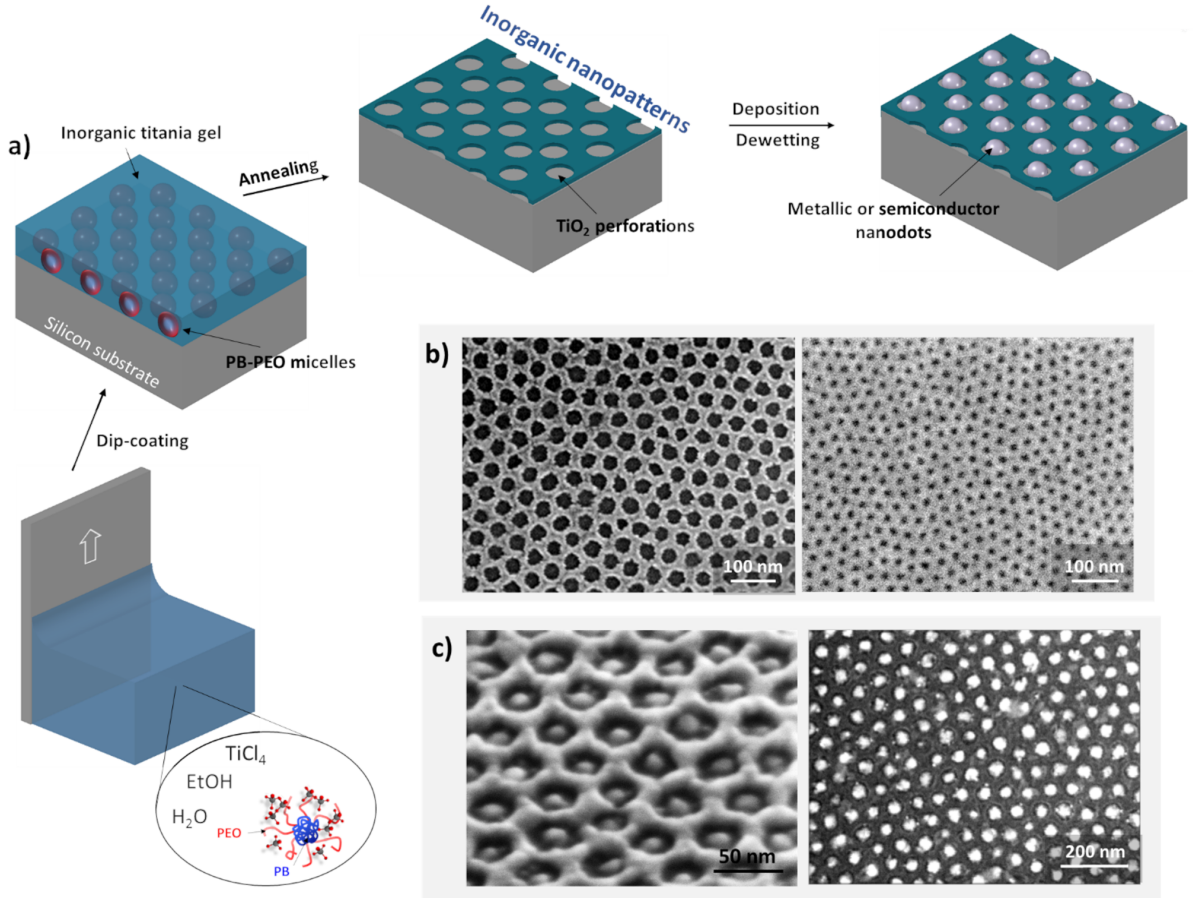

Figure 1: a) Scheme representing the process used to obtain organized metallic or semiconductor nanodots. A monolayer of micelles embedded in a titania gel is first deposited on a silicon substrate. After annealing, TiO_2 inorganic nanopatterns are formed revealing the bare silicon. In the appropriate conditions (discussed later), a single nanodot per perforation is obtained. b) SEM images of the TiO_2 INPs network after annealing for: (left) large perforations of 20 nm ($PB_{12.5}-$b-PEO_{15}), (right) small perforations of 12 nm ($PB_{5.5}-$b-PEO_{30}). c) SEM images of nanodots hexagonally arranged in TiO_2 INPs: (left) monocrystalline Ge nanodots and (right) Au nanodots.

(center-to-center). Thickness of the INPs was measured to be 7 nm with a refractive index $n_\lambda = 1.66 + 0.05/\lambda^2$, lower than bulk TiO_2 as expected for a perforated layer. Smaller perforations (12 ± 2) nm (spacing ≈ 30 nm) can be obtained with a smaller block copolymer (i.e. $PB_{5.5k}-$b-PEO_{30k}).

The topography and/or the chemical potential affinities between the deposited inorganic layer and the bare surface of the substrate underneath will be used to obtain perfectly organized metallic or semiconductor nanodots (Figure 1c). A careful tuning of the process

parameters, from sample preparation to post-annealing treatments, is necessary to control the INP structure.

3.1 Removal of the native silicon oxide layer

The substrate surface, accessible through the perforations, is silicon dioxide (SiO_2) originating from the INPs formation process. To remove the oxide layer, typically of a thickness of about 2 nm, the substrates are immersed into a solution of diluted HF ($1.17\,mol\,l^{-1}$) for 20 seconds. The duration is optimized to remove the silicon oxide thickness without damaging the INPs. Indeed, titania is also dissolved by HF but at a lower speed than SiO_2. Besides, the resistance of TiO_2 to HF is highly dependent on the INP annealing temperature. Figure 2 shows that for a 30 min annealing at 350 °C, the INPs are totally removed after a HF treatment of 20 seconds. Only partial damages are visible on the INPs network after a similar treatment at 400 °C whereas no damage can be seen for an annealing at 450 °C. Crystallization in anatase of sol-gel based titania is known to start at 300 °C while extended crystal grow occurs at higher temperature through diffusive sintering.[39,45] A high degree of crystallinity (larger grains with lower density of grain boundary) is thus necessary to sustain the HF treatment applied to remove the silica native layer. However, even in these conditions, if the etching duration exceeds 40 seconds, the INPs network is totally removed from the surface, likely due to the attack of the SiO_2 layer underneath the INP network, triggering its lift-off. Once the oxide layer is removed from the inside of the perforations, the substrates are immediately placed under vacuum in order to avoid the oxidation of the bare silicon surface. At this point, the diameter of the perforations is measured to be (28 ± 4) nm.

3.2 Optimization of Ge deposition parameters

In order to use the titania perforation as a template for Ge nanodots localization, the MBE deposition process consists in three steps (see Figure 3).

First, a pre-deposition annealing ("Flash": 450 °C for 20 min) is used in order to promote

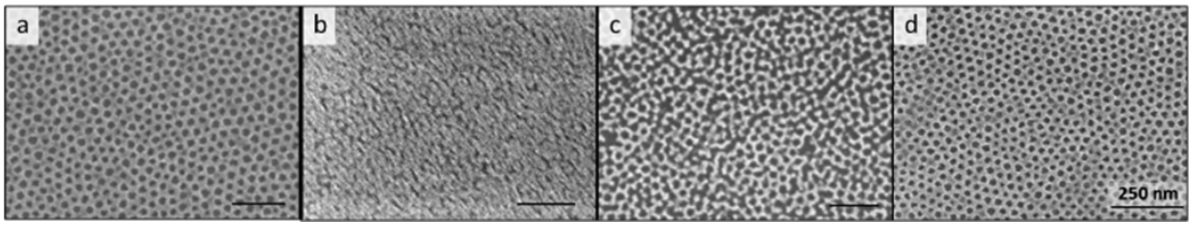

Figure 2: SEM images of INPs surfaces: (a) before HF etching and (b-d) after immersion in HF ($1.17\,\mathrm{mol\,l^{-1}}$) for 20 seconds. The INPs were calcined at 350 °C (b), 400 °C (c) and 450 °C (d) for 30 min before HF treatment.

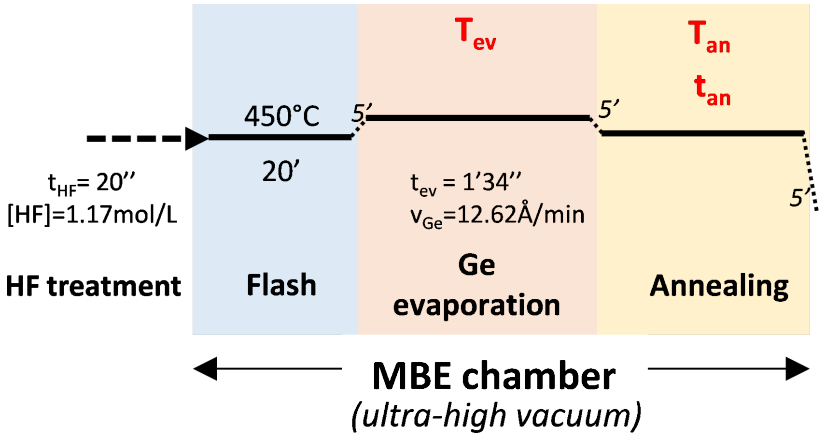

Figure 3: Scheme representing the process parameters of the Ge MBE deposition. Parameters that are varied during the study are written in red. After HF treatment, the substrate is introduced in the chamber. A flash thermal treatment is systematically performed to remove impurities, followed by Ge evaporation at a substrate temperature T_{ev}, followed by an annealing of the deposited layer at a temperature T_{an} and a duration t_{an}.

surface impurities desorption. This stage leads also to the transformation of anatase TiO_2 into rutile as deduced from subsequent XRD analysis. Even if the transition from anatase to rutile is generally expected above 600 °C for thin films,[45] ultra-high vacuum conditions promotes the diffusion enough to lead to this transition at a temperature as low as 450 °C. Then, 2 nm of Ge is deposited at a substrate temperature T_{ev}. Finally, the substrate is annealed at a temperature T_{an} during t_{an}, to facilitate dots ripening.

The deposition temperature T_{ev} promote the diffusion of adatoms. This diffusion can be limited by the surface roughness and the energetic barriers associated. In this case, nanodots nucleation centers will correspond to local energetic minima. They can be located on the titania layer. To allow the diffusion of the adatoms to the absolute energetic minima position

(bare silicon in titania layer perforation), T_{ev} must be high enough.

To assess the state of the surface after germanium deposition, the number of Ge nanodots in the perforations (N_1^{Ge}) and on the titania (N_2^{Ge}) is evaluated on SEM images. For a given area, covering at least 150 dots for each measurement, the percentage of coverage ($\%_{\mathrm{cov}} = N_1^{\mathrm{Ge}}/(N_2^{\mathrm{Ge}} + N_1^{\mathrm{Ge}})$) is calculated. If nanodots are only found in the perforations, $\%_{\mathrm{cov}} = 100\,\%$. Different deposition conditions are investigated (see Table 1) and results are summarized in Figure 4.

Table 1: Resulting placement of the nanodots for various growth temperature T_{ev} during the deposition of 2 nm of germanium, followed by different annealing conditions (temperature T_{an}, duration t_{an}). Letters in the first row corresponds to the SEM images in Figure 4.

	a	b	c	d	e
T_{ev}	20 °C	20 °C	20 °C	450 °C	650 °C
T_{an}	450 °C	450 °C	650 °C	650 °C	650 °C
t_{an}	20 min	2 h	20 min	20 min	20 min
$\%_{\mathrm{cov}}$	55 %	64 %	58 %	78 %	100 %

In all the investigated samples, one dot per perforation is always found while the number of dots found on the titania surface is variable. At room temperature deposition ($T_{\mathrm{ev}} = 20\,°\mathrm{C}$), almost as many dots are found on the INPs network than in the perforations (sample a). The effect of the post-deposition annealing treatment is weak. For $T_{\mathrm{an}} = 450\,°\mathrm{C}$, increasing annealing time from 20 min to 2 h (sample b), only increase coverage ratio from 55 % to 64 %. Besides, for $t_{\mathrm{an}} = 20\,\mathrm{min}$, increasing the annealing temperature T_{an} to 650 °C (sample c) leads to 58 % coverage. These experiments demonstrate that Ge adatoms can not overcome energetic barriers at room temperature, and nucleates on local energetic minima. Moreover, once nanodots are formed, they are stable: no ripening is observed during post-deposition annealing.

In order to promote the placement of the dots solely in the perforations, a higher deposition temperature is required. For $T_{\mathrm{ev}} = 450\,°\mathrm{C}$ (sample d) a coverage of 78 % is obtained. A perfect coverage of 100 % is found for $T_{\mathrm{ev}} = 650\,°\mathrm{C}$ with Ge dots only in the perforations (see Figures 1c and 4e). This result shows that the mobility of germanium can only be promoted

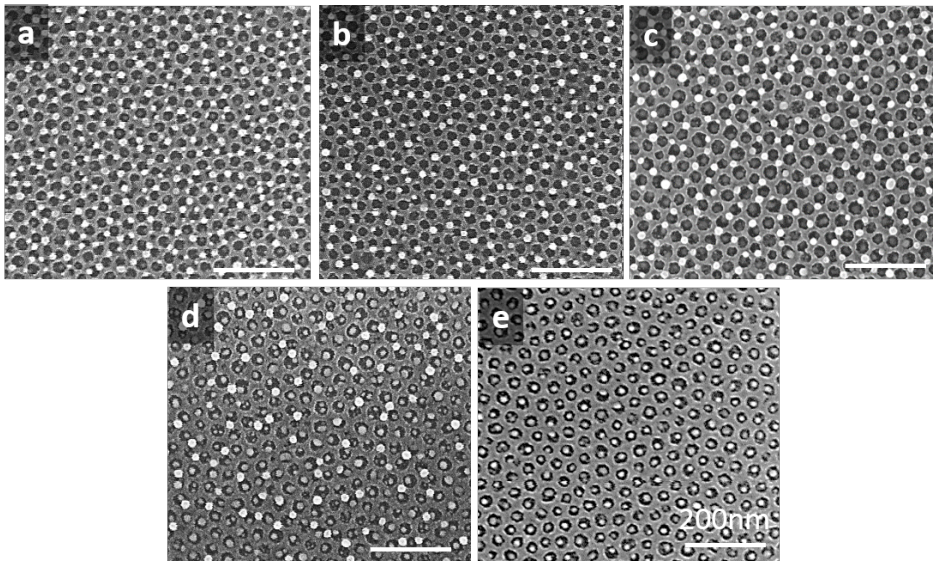

Figure 4: SEM images of the TiO_2 INPs surface after the deposition of 2 nm of germanium in various conditions summarized in Table 1.

during the nucleation step, before the formation and growth of Ge crystals on TiO_2. Above a threshold temperature, germanium can overcome the energetic diffusion barriers of TiO_2 surface, allowing the diffusion of Ge adatoms towards Si: nanodots nucleation occurs inside the perforations.

This process is probably assisted by the morphological evolution of the titania layer. Increasing the temperature, the number of defects on the TiO_2 INPs decreases: TiO_2 crystallites grow in size through diffusive sintering which reduce the number of grains boundaries and the overall number of defects.

3.3 Advanced characterization of Ge dots

The perfect disposition of Ge nanodots is driven by the germanium affinity for the Si substrate. This result suggests that the SiO_2 underlayer formed during titania deposition, is totally dissolved by the HF acid etching, inside TiO_2 perforation. Therefore, an epitaxial relationship is expected between germanium and silicon lattices. It has been investigated by XRD and HRTEM.

The XRD analysis is shown in Figure 5. As no detectable diffraction peaks were obtained

in Bragg-Brentano geometry, only GIXRD is shown. This indicates either very few crystallized volume or highly textured film (preferred crystallographic orientation along specific directions). GIXRD reveals the presence of diffraction peaks only around $2\theta = 55°$; the peak intensities depend on both the in-plane (φ) and incident angle (ω). The inset in Figure 5 is a schematic view of the GIXRD geometry. To observe the diffraction peaks of silicon and germanium in GIXRD, several points have to be taken into account: (i) in this configuration, at $\varphi = 0°$, the in-plane orientation of the Si (1 0 0) substrate is along the [0 1 0] direction; in a cubic system, the (3 1 1) planes are thus at $\varphi = 45°$. (ii) In a cubic system, the angle between the (1 0 0) and (3 1 1) planes is $\alpha = 25.24°$. (iii) The theoretical 2θ angle for (3 1 1) reflections is $2\theta = 53.68°$ for relaxed Ge and $2\theta = 56.12°$ for relaxed Si. Considering the GIXRD geometry, the corresponding diffraction peaks should appear for incident angles of $\omega = 1.6°$ for Ge (3 1 1) and $\omega = 2.8°$ for Si (3 1 1). GIXRD measurements were thus recorded with ω around 1.5° and $\varphi = 45°$ in order to detect the (3 1 1) planes. Experimentally, Figure 5 clearly shows that the diffractions peaks are only visible around $2\theta = 55°$ and that the diffraction peaks disappear when the sample is rotated in plane ($\varphi \neq 45°$) as expected for an heteroepitaxial system. Moreover, Ge (3 1 1) peak detection is optimized at $\omega = 1.6°$. Concerning the Si (3 1 1) Bragg reflection, it is also detectable at incident angle of $\omega = 1.6°$ due to the X-Ray beam average divergence and the huge substrate signal. At $\omega = 2.8°$, the Si (3 1 1) reflection is optimized and the peak at $2\theta = 54.1°$ corresponds to an average between the Ge (3 1 1) and TiO_2 (2 1 1) reflection, these peaks being clearly dissociated when the incident angle is 1.6°. This analysis thus confirms the unique Ge crystallite orientation, with (1 0 0) plane parallel to the Si substrate (1 0 0) plane. However, the experimental resolution does not allow determine the possible strain induced by the epitaxial relationship. Depending on the presence of dislocations, the germanium lattice can be either in a tensile strain or relaxed.

HRTEM analyses were performed in order to confirm the epitaxial relationship between Ge dots and the silicon substrate, but also to research the presence of structural defects at the Si-Ge interface (see Figure 6). Ge dots are in epitaxy on the silicon wafer, inside the

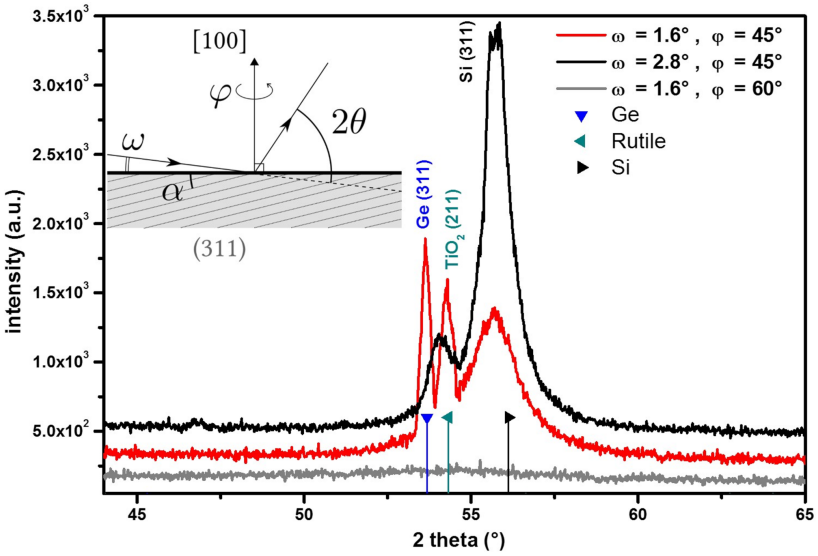

Figure 5: XRD analysis of TiO_2 INPs bearing Ge nanocrystals: patterns recorded in GIXRD geometry with two different incident (ω) and in plane (φ) angles (in plane angle is measured from the Si substrate [0 1 0] direction). The triangle markers indicate the theoretical positions of Bragg reflections related to Ge, rutile TiO_2 and Si phases around $2\theta = 55°$.

perforations, in agreement with XRD analysis. On either side, the rutile TiO_2 crystallites of the INPs are present, with the underlying thin SiO_2 layer. At the location of the Ge dot, in the perforation, the atomic lattice of Ge is seen to extend up to the crystalline surface of silicon. The monocrystalline nature of germanium is clearly visible and confirmed by Fourier Transformation. Moreover, facets are visible with no apparent defects confirming the perfect hetero-epitaxy of the Ge nanocrystals on silicon, and the tensile strain induced by the silicon substrate.

3.4 Variation in the INPs network parameters: smaller perforations

Finally, to prove the flexibility of the proposed inorganic nanoperforations, deposition of germanium was performed on TiO_2 INPs bearing smaller perforations. To obtain such pre-patterned surfaces, the same protocol was followed with a smaller block copolymer: $PB_{5.5k}-$b-PEO_{30k}. The well-ordered perforated network is visible as seen for the larger perforations (see Figure 1b). The mean diameter, deduced from SEM, is (12 ± 2) nm. Deposition was carried out following the procedure optimized for larger perforations (HF treatment

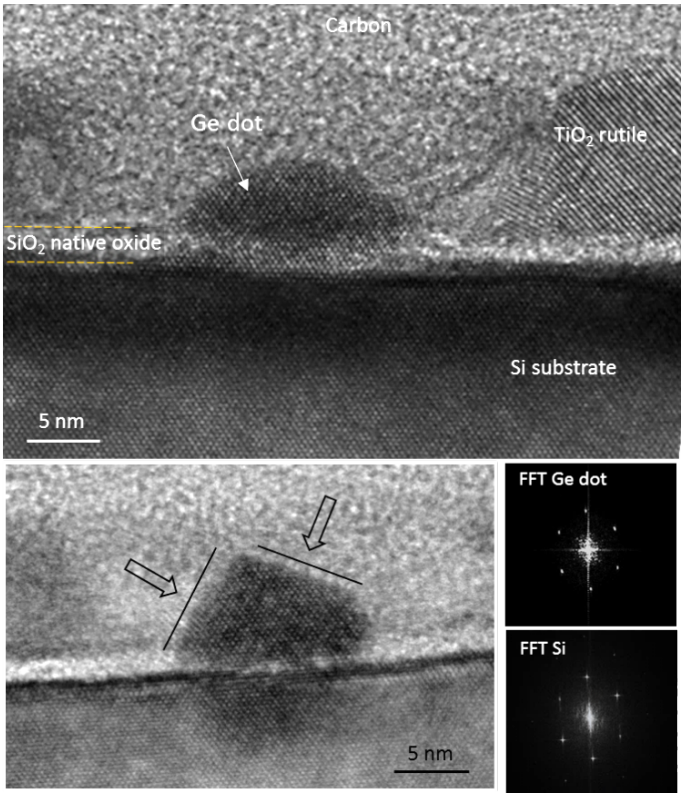

Figure 6: TEM analysis of Ge dots in TiO_2 perforations with corresponding Fourier Transform. Facets are easily visible on the Ge crystals.

20 s, 2 nm of Ge deposited at 650 °C then annealing at 650 °C for 20 min). SEM imaging after deposition shows that one Ge crystal is found in each perforation with a few large Ge dots visible on the TiO_2 network (Figure 7a). This corresponds to a $\%_{cov} = 92\,\%$. Thus, it seems that in the case of smaller perforations, a deposition at a temperature of 650 °C does not give enough mobility to Ge in order to diffuse entirely towards the perforations even if the inter-distance between perforations is smaller. The temperature was then gradually increased until no dots were found on the INPs surface. At a temperature of 800 °C, the INPs network starts to lose organization with a collapse of the INPs structure due to extensive diffusive sintering (Figure 7c). Ge dots, originally located in the perforations, merge to form larger dots as the TiO_2 topographical barrier is breaking apart. We note that, in this case, no Ge dots are found on the INPs.

A narrow window thus seems to exist with full organization of germanium in the perfora-

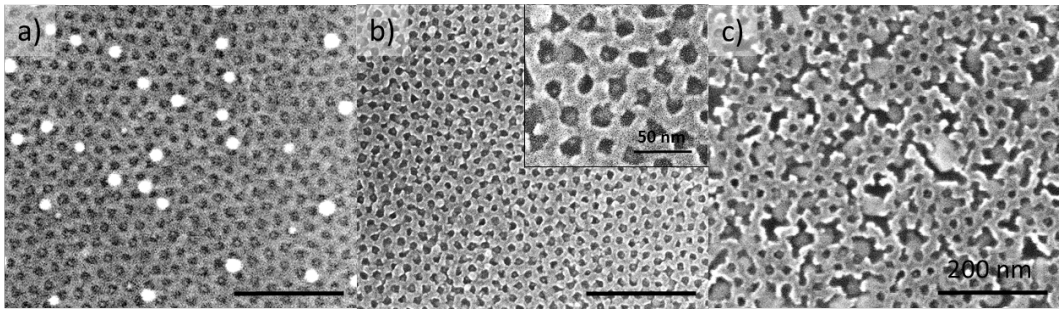

Figure 7: SEM images of the TiO_2 INPs after the deposition of 2 nm of germanium at different temperatures: a) deposition at 650 °C, b) deposition at 775 °C and c) deposition at 800 °C. No annealing is performed after deposition. The scale bar is 200 nm.

tions before the TiO_2 INPs become unstable. Results of deposition at 775 °C show organized Ge dots with full diffusion in the perforations (Figure 7b). The TiO_2 network begins to collapse but the extent is not large enough to allow the Ge dots to merge. In this case, a percentage of coverage of 98 % is found with very few dots on the INPs. The average diameter of the dots on the INPs is about the same than the ones in the perforations in contrast with the previous case (Ge deposition at 650 °C). The very small size of the Ge dots embedded in the perforations did not allow to obtain SEM images with sufficient resolution to extract a size distribution. Nevertheless, as Ge crystals are located within the INPs perforations, their size diameter is bound to be smaller than the one of the perforation ((12 ± 2) nm) and can be roughly estimated to (9 ± 3) nm. Note that, in the case of smaller perforations, the annealing step after evaporation (see scheme Figure 3) was suppressed from the process as similar results were obtained with or without post-annealing. Since the temperature is maintained for a shorter time, this allows to work at higher temperature without damaging too much the INPs.

3.5 Comparison spontaneous/directed deposition

If deposition takes place on a non-patterned surface, randomly dispersed islands with a large size distribution are expected (Figure 8a). For instance, the deposition of a 2 nm thick layer of germanium (at 650 °C under ultra-high vacuum and annealed at 650 °C for

20 min) on bare silica gives Ge dots of an average diameter of 40 nm with a very large diameter distribution ranging from 10 nm to 65 nm (Figure 8d). To direct the Ge atoms diffusion and reduce size distribution, pre-patterning of the surface is thus necessary. In our case, deposition and annealing is carried out on inorganic nanopatterns. Without any additional treatment, Ge nanodots feature a narrower size distribution than for spontaneous deposition (Figure 8b). An average diameter of (23 ± 10) nm is reported in accordance with previous studies.[19] Indeed, with this additional surface texturation, the presence of energetically favorable points leads to a more homogeneous size distribution with respect to the spontaneous deposition case. However, even if the size distribution is drastically reduced compared to a flat surface, no precise spatial organization is found. In order to obtain a precise organization of the dots, the position of defects must be controlled, which could be the case with the INPs network as it bears organized perforations. Nevertheless, without any additional treatment, the bottom of the perforations still consist of silicon oxide, which displays a low affinity with germanium. In fine, Ge nanodots will preferably nucleate on the TiO_2 INPs network where defects, such as grain boundaries between rutile crystals, will locally increase the surface energy, providing narrow size distribution but no organization.

In contrast, with the appropriate HF chemical etching, the silicon oxide can be eliminated from the bottom of the perforations revealing the silicon surface while keeping the TiO_2 structure intact (Figure 2). Silicon is a convenient nucleation point for Ge growth since Ge is highly miscible in Si. Taking advantage of the chemical heterogeneity brought by the TiO_2 INPs and in optimized deposition conditions discussed above, nucleation and growth of Ge nanodots can be controlled leading to one dot per perforation (Figure 8c). A sharp size distribution of (17 ± 2) nm is found without any dot on the INPs network. Ge nanocrystals, in epitaxy with the silicon substrate, are well organized in a hexagonal lattice with their diameter and spacing defined by the INPs network parameters.

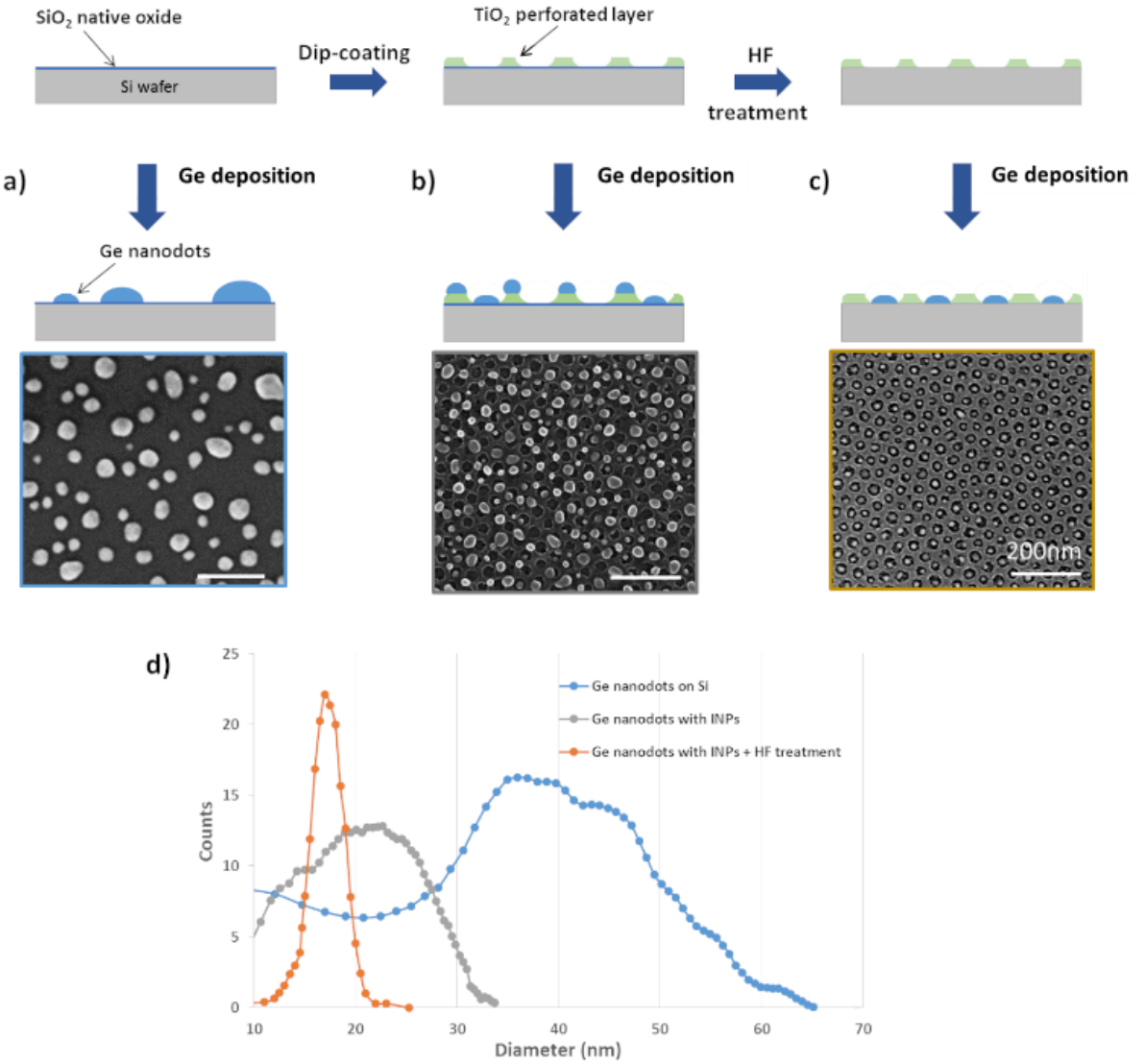

Figure 8: Deposition and dewetting of 2 nm of Ge at 650 °C followed by annealing at 650 °C for 20 min on a) a bare silicon surface, b) TiO_2 INPs without chemical etching, c) TiO_2 INPs after appropriate etching. d) Size distribution in diameter of Ge nanodots after deposition in different conditions, deduced from image analysis.

3.6 Organization of Au nanoparticles

TiO_2 INPs are now used as a pre-pattern surface for the organization of metallic nanoparticles. For this purpose, a thin gold layer of 3.5 nm is deposited by sputtering on the TiO_2 nanoperforated layer. Even before annealing, the gold layer broke down into islands of various size and shape that cover the entire substrate (Figure 9a). This is expected as the mobility of metals is higher than the one of semiconductors. The presence of the TiO_2 net-

work can be guessed with smaller islands inside the perforations and large elongated islands on the network.

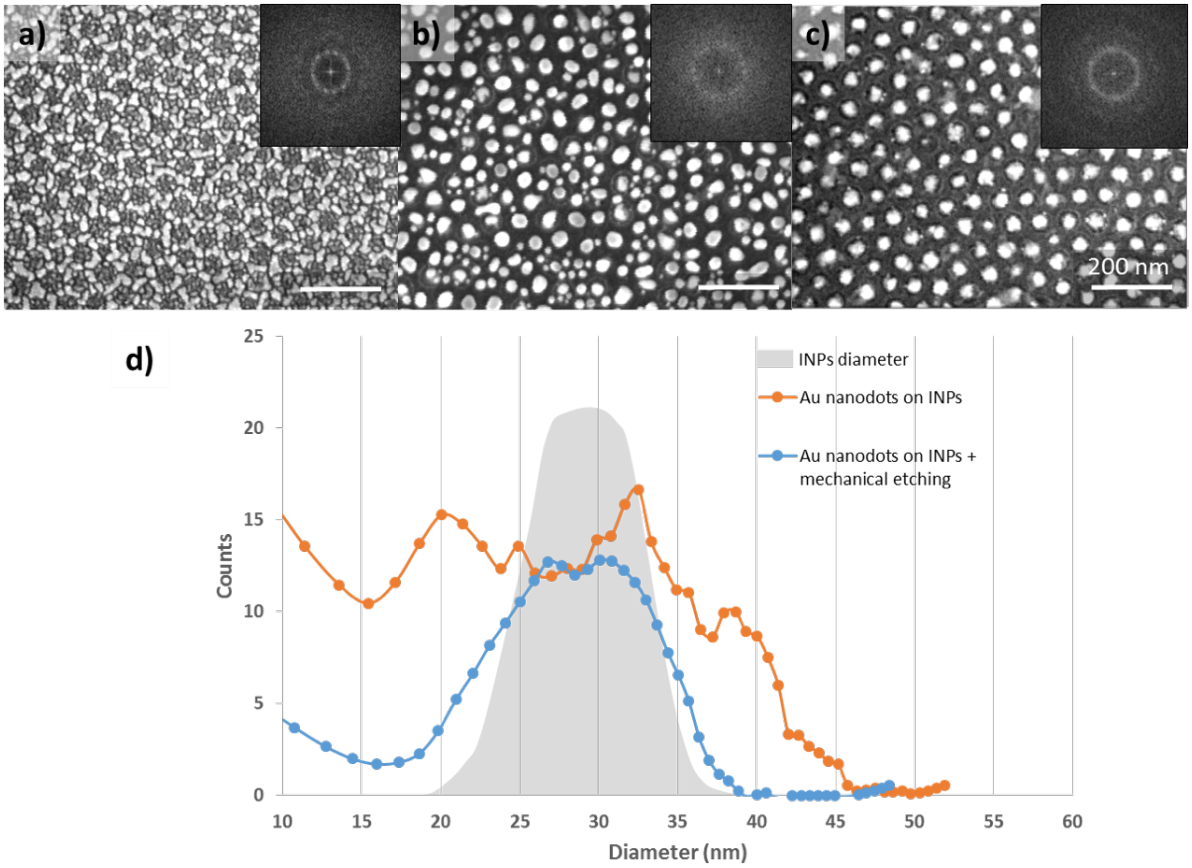

Figure 9: SEM images of a) TiO_2 INPs after the deposition of a thin Au layer, b) TiO_2 INPs with Au droplets after annealing at 450 °C for 30 min in ultra-high vacuum, c) TiO_2 INPs with Au droplets after annealing and mechanical etching. Insets display the corresponding Fourier Transformation. d) Distribution of the Au dots diameter after annealing, before and after mechanical etching.

In order to obtain more homogeneous Au domains, an annealing step is performed in an epitaxy chamber under ultra-high vacuum ($P = 10^{-10}$ Pa) at 450 °C for 30 min. In those conditions, Au thin layers are known to dewet and form isolated islands.[10] The film after annealing shows round gold droplets confirming the high mobility of gold at this temperature (Figure 9b). A large size distribution of the Au dots is found with size ranging from 10 nm to 45 nm (Figure 9d). Moreover, dots are randomly arranged without any specific interaction with the bottom of the perforations (silicon) or with the INPs network (TiO_2). This is due

to the fact that Au does not have a specific affinity for silicon compared to TiO_2. In this case, only topographical defects are directing the atomic diffusion, which is not sufficient to directly obtain organized arrays of dots in contrast with germanium deposition process. As ordering of Au dots could not be obtained solely via deposition and annealing, abrasion of the surface by gently polishing with a fabric revealed to be efficient to remove the dots on the TiO_2 without impacting those formed within the perforations. Indeed, as gold has a poor affinity for the surface, it can be easily removed mechanically. By polishing the surface, only the raised areas will be impacted: the Au dots on top of the INPs. In this case, the INPs network behave as a topographical mask that selectively protect the Au dots in the perforations. Figure 9c presents the image of the surface where only Au dots in the perforations are left after polishing with clean room paper with a force of $0.75\,\mathrm{N\,cm^{-2}}$. Nice organization with hexagonal arrangement is found corresponding to the INPs network parameter as confirmed by Fourier Transformation (FT). The size distribution of the Au dots after such mechanical treatment is $(28 \pm 5)\,\mathrm{nm}$ in diameter which is in good agreement with the size of the perforations (Figure 9d). The slight broadening towards smaller dots can be explained by the fact that not all the perforations are fully filled by gold. For comparison, if deposition of a thin Au layer is performed on bare silicon, a very large size distribution with dots of diameter about roughly thirty times the Au deposited thickness is found.[10] In the present case of a 3.5 nm Au layer, this translates into droplets of about $(100 \pm 50)\,\mathrm{nm}$ in diameter. Furthermore, in the case of metals, as only a topographical control is used, HF chemical treatment is not compulsory to organize the Au dots. However, revealing the silicon surface at the bottom of the perforations is important to have an interface between gold and silicon for instance in the case Au dots are further used as VLS catalysts to obtain out of plane nanowires. In addition, such surfaces are expected to be interesting for Surface Enhanced Raman Scattering (SERS) due to their unique organization.

4 Conclusion

TiO_2 inorganic nanopatterns proved to be an exceptional pre-templated surface for the directed ordering of both semiconductor and metallic nanodots. In the case of germanium thin layers, selective epitaxy of Ge on the bare silicon within the perforations allowed to organize the Ge nanodots after HF chemical treatment and in optimized deposition conditions. Highly organized sub-100 nm germanium nanocrystals were obtained in epitaxy, with a sharp size distribution. This is a huge improvement compared to stochastic nucleation of Ge on Si. Next, TiO_2 INPs were also exploited to control gold deposition. With an appropriate polishing of the surface, gold nanodots were obtained in an organized fashion with a narrow size distribution. Furthermore, we proved that the density and organization of the nanodots can be easily tailored by changing the INPs network parameters.

Acknowledgement

The authors acknowledge the funding by A*MIDEX (reference. ANR- 11-IDEX-0001-02) and MATISSE, the facilities of the NANOTECMAT platform at the IM2NP and of the CP2M of Aix-Marseille University.

References

(1) O'Regan, B.; Grätzel, M. A low-cost, high-efficiency solar cell based on dye-sensitized colloidal TiO2 films. *Nature* **1991**, *353*, 737–740.

(2) Aberg, I.; Vescovi, G.; Asoli, D.; Naseem, U.; Gilboy, J. P.; Sundvall, C.; Dahlgren, A.; Svensson, K. E.; Anttu, N.; Bjork, M. T.; Samuelson, L. A GaAs nanowire array solar cell with 15.3% efficiency at 1 sun. *IEEE Journal of Photovoltaics* **2016**, *6*, 185–190.

(3) Tian, B.; Zheng, X.; Kempa, T. J.; Fang, Y.; Yu, N.; Yu, G.; Huang, J.; Lieber, C. M.

Coaxial silicon nanowires as solar cells and nanoelectronic power sources. *Nature* **2007**, *449*, 885–889.

(4) Dasary, S. S.; Singh, A. K.; Senapati, D.; Yu, H.; Ray, P. C. Gold nanoparticle based label-free SERS probe for ultrasensitive and selective detection of trinitrotoluene. *Journal of the American Chemical Society* **2009**, *131*, 13806–13812.

(5) Shiraki, Y.; Sunamura, H.; Usami, N.; Fukatsu, S. Formation and optical properties of SiGe/Si quantum structures. *Applied Surface Science* **1996**, *102*, 263–271, Ref pour 3D dots arrays used in optoelectronics.

(6) Yakimov, A. I.; Dvurechenskii, V. A.; Kirienko, V. V.; Yakovlev, Y. I.; Nikiforov, A. I.; Adkins, C. J. Long-range Coulomb interaction in arrays of self-assembled quantum dots. *Phys. Rev. B* **2000**, *61*, 10868–10876, Ref pour 3D dots arrays used in electronics.

(7) Choi, W. K.; Liew, T. H.; Chew, H. G.; Zheng, F.; Thompson, V. C.; Wang, Y.; Hong, M. H.; Wang, X. D.; Li, L.; Yun, J. A combined top-down and bottom-up approach for precise placement of metal nanoparticles on silicon. *Small* **2008**, *4*, 330–333, Patterning of resist by laser interference for selective removal of SiO2. Deposition of Au on Si (in solution) and removal of the rest of the layer (on SiO2). Dots size centered around 30,60,95 nm.

(8) Zhang, X.; Qiao, Y.; Xu, L.; Buriak, J. M. Constructing metal-based structures on nanopatterned etched silicon. *ACS Nano* **2011**, *5*, 5015–5024, Patterning by deposition of PS-PVP then removing of PVP and HF etching to create nanopatterns Filling of the nanopatterns by TiO2 and by Gold gold diameter about 30nm no application in VLS.

(9) Altomare, M.; Nguyen, N. T.; Schmuki, P. Templated dewetting: designing entirely self-organized platforms for photocatalysis. *Chemical Science* **2016**, *7*, 6865–6886.

(10) Benkouider, A.; Ronda, A.; David, T.; Favre, L.; Abbarchi, M.; Naffouti, M.; Osmond, J.; Delobbe, A.; Sudraud, P.; Berbezier, I. Ordered arrays of Au catalysts by

FIB assisted heterogeneous dewetting. *Nanotechnology* **2015**, *26*, 505602, Au dewetting by Malek Best dewetting conditions: 600C/30min.

(11) Nitta, Y.; Shibata, M.; Fujita, K.; Ichikawa, M. Nanometer-scale Ge selective growth on Si (001) using ultrathin SiO film. *Surface Science Letters* **2000**, *462*, Thin oxide on silicon selectively removed by Ebeam from STM tip. Selective deposition of ge from GeH4.

(12) Leroy, F.; Eymery, J.; Gentile, P.; Fournel, F. Controlled surface nanopatterning with buried dislocation arrays. *Surface Science* **2003**, *545*, 211–219, Nanopatterning of Ge by misfit dislocations.

(13) Berbezier, I.; Ronda, A.; Portavoce, A.; Motta, N. Ge dots self-assembling: Surfactant mediated growth of Ge on SiGe (118) stress-induced kinetic instabilities. *Applied Physics Letters* **2003**, *83*, 4833–4835, Ge dots by growth on vicinal SiGe instabilities on Si.

(14) Essolaani, W.; Picaud, F.; Ramseyer, C.; Gambardella, P.; Saïd, M.; Spanjaard, D.; Desjonquères, M. C. Formation of one-dimensional ordered alloy at step edges: An atomistic study of the (2 x 1) Ni/Pt alloy on the Pt(997) surface. *Surface Science* **2011**, *605*, 917–922.

(15) Pascale, A.; Berbezier, I.; Ronda, A.; Videcoq, A.; Pimpinelli, A. Self-organization of step bunching instability on vicinal substrate. *Applied Physics Letters* **2006**, *89*, 21–24.

(16) Berbezier, I.; Ronda, A. Self-assembling of Ge dots on nanopatterns: Experimental investigation of their formation, evolution and control. *Physical Review B - Condensed Matter and Materials Physics* **2007**, *75*, 1–10.

(17) Spinelli, P.; Verschuuren, M. a.; Polman, A. Broadband omnidirectional antireflection coating based on subwavelength surface Mie resonators. *Nature communications* **2012**, *3*, 692.

(18) Masuda, H.; Fukuda, K. Ordered metal nanohole arrays made by a two-step replication of honeycomb structures of anodic alumina. *Science* **1995**, *268*, 1466–1468, Electrochemically self-organised surfaces on Al.

(19) Rowell, N. L.; Lockwood, D. J.; Amiard, G.; Favre, L.; Ronda, A.; Berbezier, I.; Faustini, M.; Grosso, D. Photoluminescence Efficiency and Size Distribution of Self Assembled Ge Dots on Porous TiO2. *Journal of Nanoscience and Nanotechnology* **2011**, *11*, 9190–9195, PL on Ge dots by Lockwood.

(20) Lockwood, D.; Rowell, N.; Barbagiovanni, E.; Goncharova, L.; Simpson, P.; Berbezier, I.; Favre, L.; Amiard, G.; Ronda, a.; Faustini, M.; Grosso, D. Photoluminescence Efficiency of Germanium Dots Self-Assembled on Oxides. *ECS Transactions* **2013**, *53*, 185–206, PL on Ge dots by Lockwood.

(21) Bublat, T.; Goll, D. Large-area hard magnetic L10-FePt nanopatterns by nanoimprint lithography. *Nanotechnology* **2011**, *22*, 5301–5307, NIL + Solid state dewetting.

(22) Wang, D.; Ji, R.; Schaaf, P. Formation of precise 2D Au particle arrays via thermally induced dewetting on pre-patterned substrates. *Beilstein Journal of Nanotechnology* **2011**, *2*, 318–326, NIL + solid state dewetting.

(23) Giermann, A. L.; Thompson, V. C. Solid-state dewetting for ordered arrays of crystallographically oriented metal particles. *Applied Physics Letters* **2005**, *86*, 1–3, Organized dewetting on inverted silicon pyramids.

(24) Abbarchi, M.; Naffouti, M.; Vial, B.; Benkouider, A.; Lermusiaux, L.; Favre, L.; Ronda, A.; Bidault, S. S.; Berbezier, I.; Bonod, N. Wafer scale formation of monocrystalline silicon-based Mie resonators via silicon-on-insulator dewetting. *ACS Nano* **2014**, *8*, 11181–11190, From Duplicate 2 (Wafer scale formation of monocrystalline silicon-based Mie resonators via silicon-on-insulator dewetting - Abbarchi, Marco; Naffouti, Meher; Vial, Benjamin; Benkouider, Abdelmalek; Lermusiaux, Laurent; Favre, Luc;

Ronda, Antoine; Bidault, Sébastien; Berbezier, Isabelle; Bonod, Nicolas) Dewetting of Si by Ebeam and FIB + application as Mie resonator.

(25) Aouassa, M.; Berbezier, I.; Favre, L.; Ronda, A.; Bollani, M.; Sordan, R.; Delobbe, A.; Sudraud, P. Design of free patterns of nanocrystals with ad hoc features via templated dewetting. *Applied Physics Letters* **2012**, *101*, 1–5, Si and Ge thin layer dewetting assisted by FIB.

(26) Karmous, A.; Cuenat, A.; Ronda, A.; Berbezier, I.; Atha, S.; Hull, R. Ge dot organization on Si substrates patterned by focused ion beam. *Applied Physics Letters* **2004**, *85*, 6401–6403, Ge dots organization by FIB.

(27) Naffouti, M.; Backofen, R.; Salvalaglio, M.; Bottein, T.; Lodari, M.; Voigt, A.; David, T.; Benkouider, A.; Fraj, I.; Favre, L.; Ronda, A.; Berbezier, I.; Grosso, D.; Abbarchi, M.; Bollani, M. Complex dewetting scenarios of ultrathin silicon films for large-scale nanoarchitectures. *Science Advances* **2017**, *3*, 1472–1482, Science advances marco Dewetting after Ebeam.

(28) Abbarchi, M. et al. Solid-state dewetting of single-crystal silicon on insulator: effect of annealing temperature and patch size. *Microelectronic Engineering* **2018**, *190*, 1–6, Details of Ebeam Science Advances.

(29) Kim, H. C.; Park, S. M.; Hinsberg, W. D.; Division, I. R. Block copolymer based nanostructures: Materials, processes, and applications to electronics. *Chemical Reviews* **2010**, *110*, 146–177, Review on lithography by block-copo self assembly.

(30) Grosso, D.; Ribot, F.; Boissiere, C.; Sanchez, C. Molecular and supramolecular dynamics of hybrid organic-inorganic interfaces for the rational construction of advanced hybrid nanomaterials. *Chem. Soc. Rev.* **2011**, *40*, 829–848, Review on micellar templated hybrid (organic/inorganic) mesophases EISA.

(31) Dimitrov, A. S.; Nagayama, K. Continuous Convective Assembling of Fine Particles into Two-Dimensional Arrays on Solid Surfaces. *Langmuir* **1996**, *12*, 1303–1311, First paper on Nanosphere lithography.

(32) Kadiri, H. Auto-organisation assistée pour la nano-impression à grande échelle et surfaces optiques multifonctionnelles. Ph.D. thesis, 2017; These sur l'autoorganisation de spheres en monocouche par dip pour la litho.

(33) Ghicov, A.; Schmuki, P. Self-ordering electrochemistry: a review on growth and functionality of TiO2 nanotubes and other self-aligned MOx structures. *Chemical Communications* **2009**, 2791.

(34) Kuemmel, M.; Allouche, J.; Nicole, L.; Boissière, C.; Laberty, C.; Amenitsch, H.; Sanchez, C.; Grosso, D. A chemical solution deposition route to nanopatterned inorganic material surfaces. *Chemistry of Materials* **2007**, *19*, 3717–3725, general method for preparation of nanopatterns different types of motifs depending on polymers added and conditions.

(35) Kuemmel, M.; Smått, J.-H.; Boissière, C.; Nicole, L.; Sanchez, C.; Lindén, M.; Grosso, D. Hierarchical inorganic nanopatterning (INP) through direct easy block-copolymer templating. *Journal of Materials Chemistry* **2009**, *19*, 3638, Hierarchical porosity with two size of block copolymer.

(36) Faustini, M.; Grosso, D. Self-assembled inorganic nanopatterns (INPs) made by sol-gel dip-coating: Applications in nanotechnology and nanofabrication. *Comptes Rendus Chimie* **2015**, 1–18.

(37) Faustini, M.; Marmiroli, B.; Malfatti, L.; Louis, B.; Krins, N.; Falcaro, P.; Grenci, G.; Laberty-Robert, C.; Amenitsch, H.; Innocenzi, P.; Grosso, D. Direct nano-in-micropatterning of TiO2 thin layers and TiO2/Pt nanoelectrode arrays by deep X-ray

lithography. *Journal of Materials Chemistry* **2011**, *21*, 3597–3603, TiO2 nanoperforations/Pt electrode.

(38) Faustini, M.; Drisko, G. L.; Letailleur, A. A.; Montiel, R. S.; Boissière, C.; Cattoni, A.; Haghiri-Gosnet, A. M.; Lerondel, G.; Grosso, D. Self-assembled titanium calcium oxide nanopatterns as versatile reactive nanomasks for dry etching lithographic transfer with high selectivity. *Nanoscale* **2013**, *5*, 984–990, CaTiO3 as mask for etching.

(39) Faustini, M.; Nicole, L.; Boissière, C.; Innocenzi, P.; Sanchez, C.; Grosso, D. Hydrophobic, antireflective, self-cleaning, and antifogging sol-gel coatings: An example of multifunctional nanostructured materials for photovoltaic cells. *Chemistry of Materials* **2010**, *22*, 4406–4413, 10nm thick with 20nm pores TiO2 on top of mesoporous (F127) SiO2 for hydrophobic, photocatalytic, antireflective coatings.

(40) Laberty-Robert, C.; Kuemmel, M.; Allouche, J.; Boissière, C.; Nicole, L.; Grosso, D.; Sanchez, C. Sol-gel route to advanced nanoelectrode arrays (NEA) based on titania gold nanocomposites. *Journal of Materials Chemistry* **2008**, *18*, 1216, Craters for nanoelecrode coating.

(41) Martínez-Ferrero, E.; Forneli, A.; Boissière, C.; Grosso, D.; Sanchez, C.; Palomares, E. Tailored 3D interface for efficiency improvement in encapsulation-free hybrid light-emitting diodes. *ACS Applied Materials and Interfaces* **2011**, *3*, 3248–3251, Craters for LED.

(42) Lepoutre, S.; Grosso, D.; Sanchez, C.; Fornasieri, G.; Rivière, E.; Bleuzen, A. Tailor-made nanometer-scale patterns of photo-switchable prussian blue analogues. *Advanced Materials* **2010**, *22*, 3992–3996.

(43) Neu, V.; Schulze, C.; Faustini, M.; Lee, J.; Makarov, D.; Suess, D.; Kim, S.-K.; Grosso, D.; Schultz, L.; Albrecht, M. Probing the energy barriers and magnetization re-

versal processes of nanoperforated membrane based percolated media. *Nanotechnology* **2013**, *24*, 145702, INP +Co/Pt.

(44) Schulze, C. et al. Magnetic films on nanoperforated templates: a route towards percolated perpendicular media. *Nanotechnology* **2010**, *21*, 5701–5710, Craters +CoPt.

(45) Louis, B.; Krins, N.; Faustini, M.; Grosso, D. Understanding Crystallization of Anatase into Binary SiO2/TiO2 Sol-Gel Optical Thin Films: An in Situ Thermal Ellipsometry Analysis. *The Journal of Physical Chemistry C* **2011**, *115*, 3115–3122, Study of the parameters in SiO2/TiO2 annealing and crystallisation.